THE EFFECT OF CRYSTALLOGRAPHIC ORIENTATION ON THE PHYSICAL AND MECHANICAL PROPERTIES OF AN INVESTMENT CAST SINGLE CRYSTAL NICKEL-BASE SUPERALLOY

R. P. Dalal, C. R. Thomas, and L. E. Dardi

Senior Development Engineer, Development Engineer, and Director, R&D, respectively, Howmet Turbine Components Corporation, Whitehall, Michigan 49461, USA.

Summary

The effect of crystallographic orientation on the 70°F to 2000°F physical and mechanical properties of <001>, <011>, <112>, and <111> oriented investment cast dendritic single crystal Ni-6.8Al-13.8Mo-6W alloy has been investigated. As expected for a cubic crystal, the thermal expansion coefficient is invariant with orientation and Young's Modulus is highest in the <111> and lowest in the <001> direction. The 70°F tensile properties of the material are anisotropic, with highest ultimate and yield strength in the <111> orientation and greatest ductility in the <011> orientation; whereas, tensile strength is essentially isotropic at 1800°F and 2000°F. The 1800°F and 2000°F creep-rupture properties of the alloy exhibit significant anisotropic behavior. Rupture life is nine times higher at 1800°F/36 ksi and sixteen times higher at 2000°F/20 ksi in the <111> orientation than in the <001> orientation. 1800°F axial strain-controlled low cycle fatigue life correlates well with simple parameters related to Young's Modulus.

Introduction

The use of nickel-base superalloy single crystals (SC) as gas turbine engine hot section components has progressed from a highly innovative concept during the 1960's (1-3) to an engineering reality in modern commercial engines (4-5). The production material in use by Pratt & Whitney Aircraft, Alloy 454, contains significant levels of chromium, aluminum, and tantalum, which produces approximately 65 vol. pct. gamma prime and is vacuum investment cast with an <001> spanwise airfoil crystallographic orientation, which imparts excellent thermal fatigue and creep-rupture resistance (4).

Recognizing that superalloy single crystals are anisotropic (1,5,6), and substantial strength levels can be achieved in alloys that contain high levels of gamma prime and refractory alloying elements, particularly molybdenum (7-10), a program was initiated during early 1979 to investigate the foundry producibility of SC articles having various controlled orientations. This work characterized the directional dependence of the physical and mechanical properties. Superalloy crystallographic orientation effects are of interest because turbine components operate in a complex state of stress. Ni-6.8Al-13.8Mo-6W alloy (herein coded SC 7-14-6) was selected for the work since it exhibits the constitutional features mentioned above, and apart from considerations of uncoated environmental resistance, appeared to represent a good model system for study.

Technical Approach

Two five hundred pound heats of SC 7-14-6 were vacuum induction melted using high purity raw materials. The melts exhibited similar chemical compositions, Table I.

Table I. Chemical Composition of SC 7-14-6 (Wt. Pct.)

Heat	Ni	Al	Mo	W	C	B	Zr
A	Bal	6.63	13.24	5.92	0.01	0.002	0.01
B	Bal	6.66	13.86	5.88	0.01	0.002	0.01
Aim	Bal	6.8	13.5	6.1	-	-	-

A variety of SC articles, including 0.6" dia. x 6" bars, 0.5" x 4" x 6" plates, and complex cored (air cooled) turbine components, were directionally-solidified in Mono-Shell® investment molds at the Austenal Dover and Misco Whitehall Divisions of Howmet. The desired <001>, <113>, <011>, <112>, and <111> primary and secondary crystallographic directions were achieved by positioning parent metal seed crystals of predetermined orientations in the mold immediately below the article cavity (11). All material was subjected to normal X-ray, fluorescent penetrant, and grain-etch inspections to assess general quality and to confirm the absence of high angle boundaries. The crystallographic orientation of each SC article was determined by Laue back reflection X-ray diffraction techniques.

Instrumented bars of each heat were exposed in a thermal gradient furnace (1400°F to 2500°F) and metallographically examined to determine solvus and incipient melting temperatures. Except for melting temperature determinations, measurements of this kind generally are repeatable to within

±5°F and accurate to within +10°F. Based on the results, the articles were solution treated at 2350°F/4h in vacuum and inert gas cooled at a rate equivalent to air cooling. Nearly all the test material then was subjected to a 1975°F/4h/AC simulated coating cycle and a 1600°F/32h/AC age. Samples of as-cast and heat treated material were characterized using optical and electron optical (SEM/EDA and TEM) techniques and a limited amount of differential thermal analysis (DTA). X-ray diffraction of 10%HCl/methanol extractions and properly oriented polished samples was employed respectively to identify microstructural constituents and to measure the γ and γ' lattice parameters.

Alloy density was determined by weight change upon water immersion (ASTM C373). The thermal expansion coefficient and the dynamic Young's and shear moduli of <001>, <011>, and <111> oriented SC 7-14-6 were measured over the temperature range from 70°F to 2000°F. The former was obtained using 0.250" dia. x 2" pins by dilatometric methods (ASTM E228-71) and the latter were determined using 0.50" x 0.10" x 2.5" samples employing sonic resonance techniques(12). The elastic constants of the material then were calculated using E <001>, E <111>, and G <001> (13).

Triplicate tensile tests at 70°F, 1400°F, 1800°F, and 2000°F, and constant load creep-rupture evaluations at 1400°F/100 ksi, 1800°F/36 ksi and 2000°F/20 ksi, of <001>, <011>, <112> and <111> oriented material were conducted in air using 0.250" dia. specimens. The rupture data, which included test durations of up to 800 hrs at 1800°F, were correlated using the Larson-Miller parameter with C=20. Axial strain-controlled 1800°F isothermal low cycle fatigue (LCF) testing of <001>, <113>, <011>, <112>, and <111> oriented material was performed in air using 0.200" dia. x 0.700" gauge length specimens employing an A ratio of 1.0 and a Haversine wave form (0.33Hz). The LCF evaluations were conducted using an MTS Model 810 closed loop servohydraulic testing machine with a 20,000 lb load frame employing induction heated specimens. Temperature was controlled using Type K thermocouples spot welded to both shoulders of the specimen and monitored continually in the gauge section using an Ircon G series optical pyrometer. Linear regression analyses of the LCF test population were performed in an effort to correlate fatigue life with simple parameters.

Representative failed mechanical property test specimens were examined using optical metallographic and SEM techniques. It should be noted that the tensile and creep-rupture evaluations were approximately split between the two heats; whereas, almost all of the LCF tests were conducted using Heat B.

Results and Discussion

As expected, the cast articles generally were high quality dendritic single crystals exhibiting crystallographic orientations that usually were within ±5° and almost invariably were within ±10° of the seed crystal axis. The alloy demonstrates excellent castability from the standpoints of foundry ceramic material (e.g., mold and core) compatibility and overall metallurgical integrity.

Microstructural Characterization

As cast SC 7-14-6 contains a dispersion of γ' ($\approx$1.5μm) in a γ matrix and approximately 3 to 5 vol. pct. of interdendritic BCC α-Mo (a_o=3.139Å),

Figure 1A. The presence of minor amounts of α-Mo in Ni-Mo alloys has been observed by Maxwell (14). The selected 2350°F (4h) solution treatment temperature produces a high degree of homogeneity, dissolves substantially all the γ' in the as-cast material while avoiding incipient melting, but is insufficient to eliminate the α-Mo phase, Table II and Figure 1B. Material in the fully heat treated condition (2350°F/4h/GFC+1975°F/4h/AC+1600°F/32h/AC) contains approximately 80 vol. pct. γ' (≈0.6μm) with a lattice parameter of 3.579Å in a γ matrix with a lattice parameter of 3.611Å.

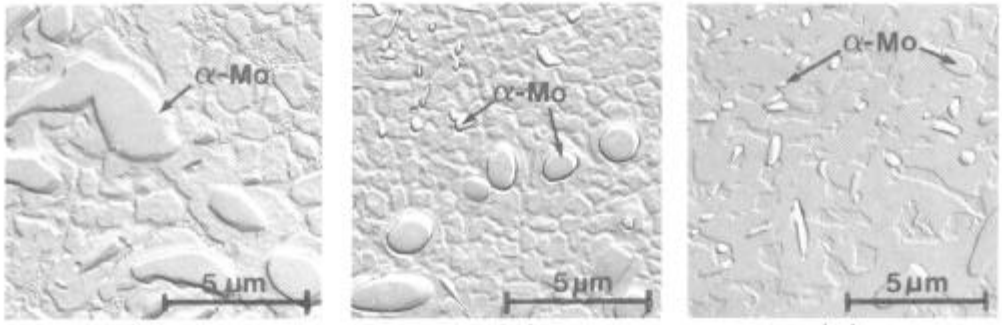

(A) (B) (C)

Figure 1 - TEM Replicas of SC 7-14-6 Alloy in As-Cast (A) and Fully Heat Treated (B) Conditions and After Rupture Testing at 1800°F for 61 hrs (C).

This represents a mismatch of -0.89% and TEM examination revealed the presence of extensive γ-γ' interfacial dislocation arrays. In addition, both as-cast and fully heat treated material have dispersed throughout the γ matrix an extremely fine precipitate which appears to be a Ni_xMo compound. In addition, the DTA traces reveal an exothermic peak at approximately 1520°F. These tentative findings appear to agree with the work of Pearson et. al. (10), who discovered extensive Ni_xMo precipitation within the γ phase of a SC Ni-5.8Al-14.6Mo-6.2Ta (wt. pct.) alloy and found that the phase goes into solution at about 1500°F.

Table II. Gradient Thermal Response of As-Cast SC 7-14-6 (°F)

Heat	γ' Solvus		α-Mo Solvus	Incipient Melting Point
	Commence	Complete		
A	2246	2330	2435	2440
B	2200	2320	2430	2435

Physical Properties

The density of SC 7-14-6 is 0.313 lbs/in^3 (8.68 gms/cm^3). Thermal expansion coefficient (TEC) is an invariant with crystallographic orientation, as expected for a cubic crystal (15), and increases with increasing temperature, Table III. The TEC of SC 7-14-6 is approximately 10 percent lower than the more conventional alloy Mar-M200 (16), perhaps as a result of its higher Mo and lower chromium content.

Table III. Mean Thermal Expansion Coefficient of SC 7-14-6 (10^{-6}/°F)
(70°F to Indicated Temperature)

Temperature (°F)	<001>	<011>	<111>	Avg.
212	4.8	3.5	3.5	3.9
392	4.9	4.0	4.9	4.6
572	5.3	4.7	4.9	4.9
756	5.5	5.1	5.4	5.3
932	5.7	5.3	5.6	5.5
1112	6.0	5.7	6.0	5.9
1292	6.4	5.7	6.3	6.1
1472	6.8	6.5	6.6	6.6
1652	7.4	6.9	7.0	7.1
1832	7.6	7.3	7.4	7.4
2012	8.0	7.7	7.7	7.7
2192	8.7	8.3	8.1	8.3

The dynamic Young's Modulus of SC 7-14-6 is highest in the <111> direction (41.3 x 10^6 psi at 70°F) and lowest in the <001> direction (19.1 x 10^6 psi at 70°F), Figure 2. It is interesting to note that although SC 7-14-6 and pure Ni single crystals (17) exhibit similar elastic anisotropy coefficients, $2C_{44}/(C_{11}-C_{12})$ (2.55 vs. 2.63 at 70°F), in SC 7-14-6 C_{44} is higher than C_{12}, Table IV. Although these results have not been confirmed, it should be noted that they are internally consistent, in that measured values of E <011> agree well with values calculated from the independent measurements E <001>, G <001>, and E <111>.

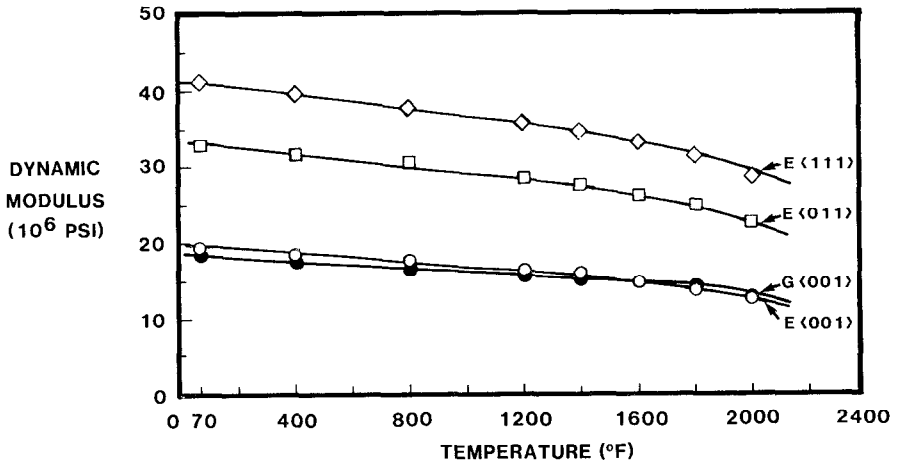

Figure 2 - Effect of Orientation on the Dynamic Modulus of SC 7-14-6.

Table IV. Elastic Constants of SC 7-14-6

TEMPERATURE (°F)	COMPLIANCE (10^{-7} PSI^{-1})			STIFFNESS (10^6 PSI)		
	S_{11}	S_{12}	S_{44}	C_{11}	C_{12}	C_{44}
70	0.523	-0.165	0.534	27.12	12.50	18.72
1400	0.637	-0.209	0.649	22.97	11.29	15.40
1800	0.735	-0.245	0.719	20.40	10.20	13.90
2000	0.813	-0.270	0.763	16.01	9.15	13.10

Tensile Properties

Consistent with its low Schmid factor for assumed (111)<$\bar{1}$01> deformation at low to intermediate temperatures (18-21), the <111> orientation generally demonstrates the highest ultimate and yield strength at 70°F and 1400°F. At elevated temperatures, where multiple slip would be expected to predominate, the tensile strength of the material is substantially isotropic, Figure 3. The <011> orientation generally displays the lowest strength and greatest ductility, and invariably exhibits elliptically deformed (initially circular cross section) test samples, which suggests that extensive single slip and lattice rotation are occurring (22). No heat-to-heat effect on tensile or creep-rupture properties was observed.

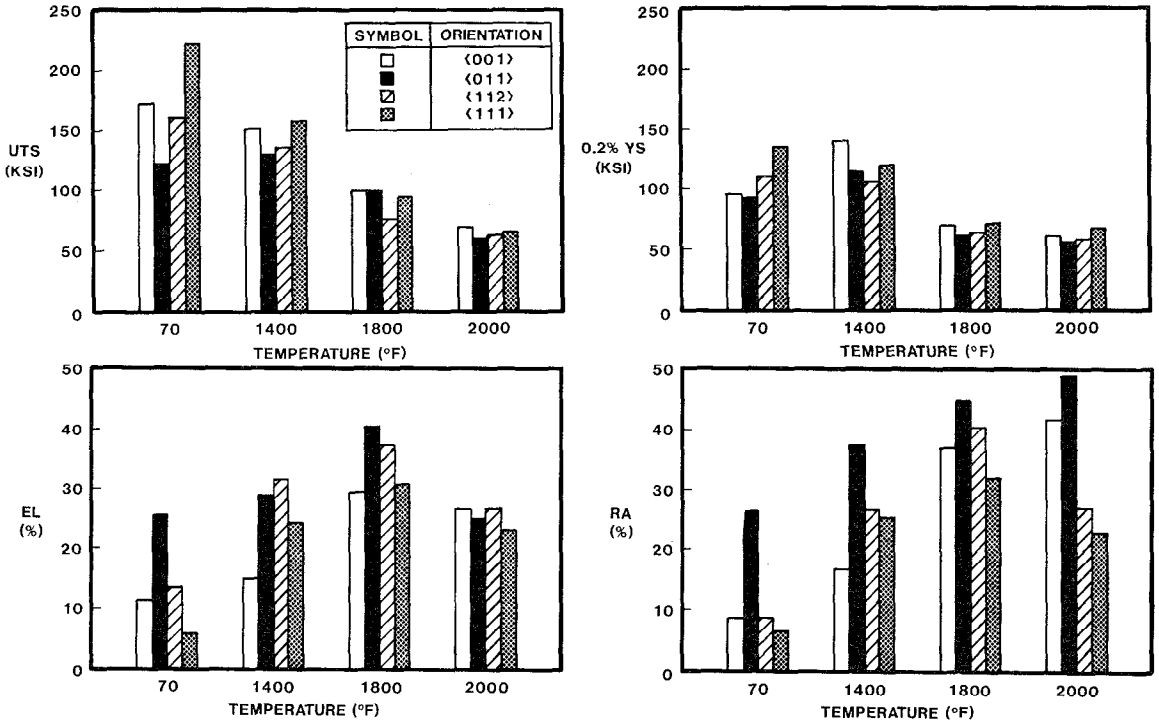

Figure 3 - Effect of Temperature on the Tensile Properties of SC 7-14-6.

Creep-Rupture Properties

SC 7-14-6 demonstrates a substantial degree of creep-rupture anisotropy at 1800°F and 2000°F, Figure 4. The <111> orientation consistently demonstrates the greatest rupture life and creep strength with usually the lowest ductility of the orientations tested. At 1800°F/36 ksi, the rupture life is a factor of nine greater (523h vs. 58h) and the time to 1% creep is a factor of forty-one greater (249h vs. 6h) than in the <001> orientation. At 2000°F/20 ksi, the respective advantages are a factor of sixteen (450h vs. 28h) and a factor of one hundred (402h vs. 4h), Table V. The reason for this unexpected level of anisotropy has not been established, but studies in progress indicate that it occurs in other alloys which have very high levels of molybdenum, tungsten, and aluminum (gamma prime).

Table V. Creep-Rupture Properties of SC 7-14-6

TEMPERATURE (°F)	STRESS (KSI)	NOMINAL CRYSTALLOGRAPHIC ORIENTATION	SPECIMEN DEVIATION (°)	RUPTURE LIFE (H)	TIME TO 1% CREEP (H)	EL (%)	RA (%)	PRIOR CREEP (%)
1400	110	<001>	2	11	0.3	30.6	30.9	24.4
		<011>	2	2	1	33.1	35.3	6.8
		<111>	2	42	0.2	47.5	18.3	27.7
	100	<001>	2	37	4	28.5	33.2	24.9
			2	57	4	28.5	36.8	24.0
				47	4	28.5	35.0	24.4
		<011>	1	9	5	10.9	28.4	2.3
			1	5	<0.1	29.4	34.8	0.5
			2	4	2	28.8	39.6	3.0
			2	4	2	39.4	34.4	7.0
			4	4	2	27.5	40.9	1.5
				5	2	27.2	35.6	2.8
		<112>	3	43	11	21.7	25.6	16.5
			5	35	6	22.8	27.7	21.9
				39	8	22.2	26.6	19.2
		<111>	2	178	3	16.0	17.6	15.1
			2	189	7	16.1	16.4	14.4
				183	5	16.1	17.0	14.7
1800	36	<001>	2	52	3	46.2	44.3	34.4
			2	49	6	47.5	42.3	27.7
			2	57	6	35.5	35.5	32.7
			3	61	7	42.2	39.8	31.0
			4	47	6	29.6	30.7	16.7
			8	85	11	22.0	29.5	20.6
				58	6	37.1	37.0	27.2
		<001>(1)	3	52	7	25.0	27.2	24.7
			3	52	9	23.5	25.9	22.0
				52	8	24.2	26.5	23.3
		<011>	1	60	17	13.5	33.2	4.1
			3	74	42	10.0	30.1	3.2
			5	55	17	24.7	48.4	5.7
			5	63	15	30.8	42.5	12.8
			5	56	22	36.8	51.7	6.5
			9(2)	159	88	8.0	24.3	3.7
				62	23	23.1	41.1	6.4
		<112>	3	125	23	17.1	23.1	13.7
			4	114	47	8.6	19.1	7.0
			6	80	20	15.1	16.9	10.8
			7	63	18	24.3	33.4	14.9
				95	27	16.3	23.1	11.6
		<111>	0	672	395	5.9	12.1	3.3
			1	844	325	4.4	8.9	3.5
			3	604	162	9.2	14.1	8.0
			3	327	35	7.4	13.9	4.4
			9	492	400	4.8	13.8	3.8
			10	347	229	4.9	9.2	3.2
			10	377	195	5.1	11.8	5.0
				523	249	5.9	11.9	4.6
2000	20	<001>	2	26	4	28.2	58.8	9.7
			2	27	4	23.7	62.8	12.5
			2	31	5	36.5	59.9	11.0
				28	4	29.4	60.5	11.0
		<011>	4	342	88	3.4	6.1	2.6
			4	422	84	3.1	5.8	2.2
				382	86	3.2	6.0	2.4
		<112>	2	262	229	3.0	5.1	1.9
			5	282	281	2.2	10.9	1.0
			5	299	195	3.1	7.3	2.0
				281	235	2.7	7.7	1.6
		<111>	1	424	370	2.6	3.7	1.7
			1	353	330	8.3	8.5	8.1
			1	574	505	3.5	2.5	2.0
				450	402	4.8	4.9	3.9

(1) Solution treated only
(2) Excluded from the average

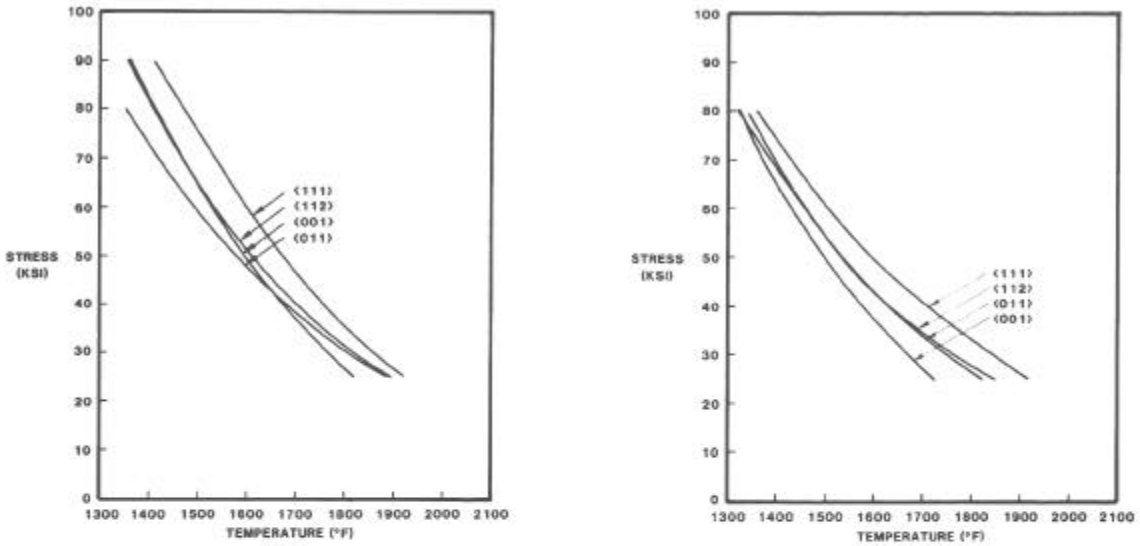

Figure 4 - Stress for 500 Hour Rupture (A) and 1% Creep (B) of SC 7-14-6.

It is also interesting to note that the <011> orientation is weaker than the <001> orientation at 1400°F (and in 70°F and 1400°F tension), but is stronger than the <001> orientation at 1800°F and 2000°F, Figure 5. All the <011> oriented creep-rupture specimens demonstrate evidence of lattice rotation, Figure 6.

Microstructural examination of the gage sections of failed creep-rupture test specimens revealed that at some time before 50 hrs under stress at 1800°F, the γ' becomes continuous in three dimensions, Figure 1C. This behavior contrasts with the γ' rafting effect which has been reported for other high misfit γ/γ' <001> oriented single crystal alloys (8-10).

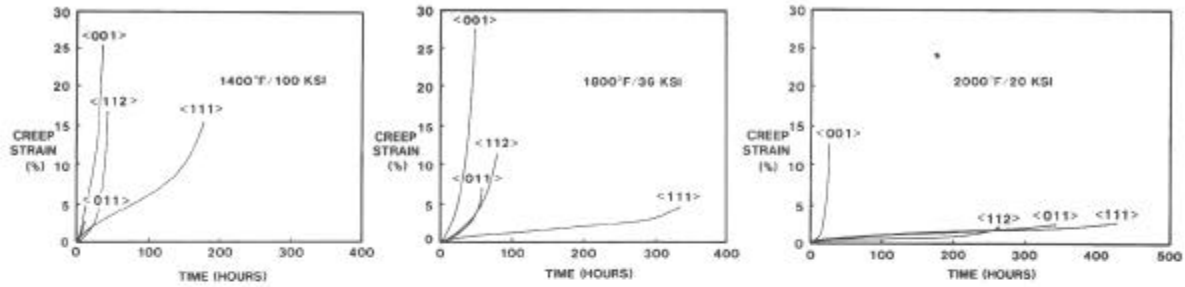

Figure 5 - Orientation Dependence of Creep Behavior of SC 7-14-6.

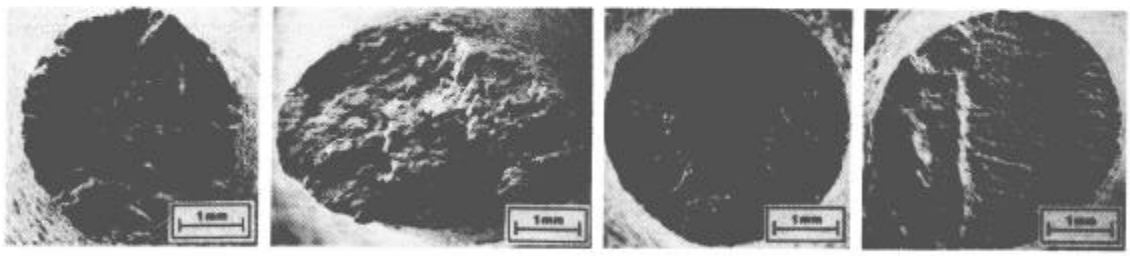

<001> <011> <112> <111>

Figure 6 - SEM Fractographs of Failed 2000°F Creep-Rupture Specimens.

Low Cycle Fatigue Properties

The axial strain controlled (A=1) LCF life of SC 7-14-6 is highest in the <001> direction, decreases with increasing Young's Modulus in a given direction, and is lowest in the <111> direction, Figure 7. All of the samples demonstrate some degree of dynamic stress-strain curve hysteresis and the amount of plastic strain increases with increasing modulus at a given total strain range, Figure 8. The cyclic plastic strain range, however, usually is less than 5% of the total strain range under all conditions evaluated, Table VI.

Table VI. 1800°F Axial Strain Controlled LCF Properties of SC 7-14-6

NOMINAL CRYSTALLOGRAPHIC ORIENTATION	SPECIMEN DEVIATION (°)	YOUNG'S MODULUS, E<hkl> (10^6 PSI)	TOTAL STRAIN RANGE, $\Delta\varepsilon_T$ (%)	ELASTIC STRAIN RANGE,(1) $\Delta\varepsilon_e$ (%)	PLASTIC STRAIN RANGE,(1) $\Delta\varepsilon_p$ (%)	TOTAL STRESS RANGE,(1) $\Delta\sigma$ (KSI)	MAXIMUM TENSILE STRESS, σ_M (KSI)	N_f (CYCLES)
<001>	2	14.6	1.0	0.93	0.06	136.33	112.0	3,985
	8	13.6	1.0	0.9	0.1	122.6	75.7	2,649
	12	14.3	0.8	0.75	0.05	106.9	93.6	12,608
		14.5	0.7	0.68	0.02	96.19	85.4	41,616
		14.4	0.6	0.58	0.016	84.07	75.6	133,615(2)
<113>		18.9	0.8	0.7	0.03	132.1	107.3	3,506
	1	18.4	0.8	0.7	0.03	139.1	115.7	1,698
	4	18.8	0.7	0.68	0.02	128.2	111.0	4,042
	8	18.8	0.6	0.57	0.03	108.7	95.1	16,532
	1	18.4	0.55	0.54	0.01	101.1	89.0	17,500
	5	19.3	0.55	0.54	0.01	101.5	88.6	17,383
	4	18.5	0.5	0.48	0.02	90.4	82.7	96,847
<011>	2	23.5	0.6	0.56	0.04	132.6	105.7	2,616
	5	24.6	0.6	0.56	0.04	136.48	107.6	3,062
	2	23.1	0.5	0.48	0.02	112.2	93.4	9,112
	4	24.7	0.4	0.39	0.01	96.71	83.4	34,063
	4	24.7	0.4	0.39	0.01	97.33	82.4	54,951
	4	23.8	0.4	0.37	0.03	97.88	85.6	47,292
	5	23.6	0.35	0.34	0.01	83.12	73.6	97,593
	2	25.1	0.3	0.29	<0.01	75.08	66.9	100,000(2)
<112>	2	26.4	0.5	0.45	0.05	121.98	101.1	3,271
	2	26.0	0.5	0.47	0.03	123.52	94.3	5,024
	5	23.1	0.5	0.48	0.02	112.24	94.3	9,112
	8	27.1	0.45	0.43	0.02	118.68	94.2	8,298
		27.3	0.4	0.39	0.01	106.9	83.6	9,665
		25.4	0.4	0.38	0.02	98.39	82.5	11,812
		26.6	0.35	0.34	0.01	92.06	76.2	33,882
	4	27.5	0.3	0.29	0.01	82.3	76.1	100,000(2)
<111>	9	31.1	0.4	0.38	0.02	122.15	91.9	2,886
	5	33.2	0.4	0.37	0.03	122.59	85.5	3,075
	8	32.8	0.4	0.39	0.01	127.7	97.5	4,652
	9	32.5	0.35	0.34	0.01	109.33	88.8	8,382
	3	31.9	0.28	0.27	0.01	88.25	79.4	55,647

(1) Taken at approximately $N_f/2$
(2) Test discontinued

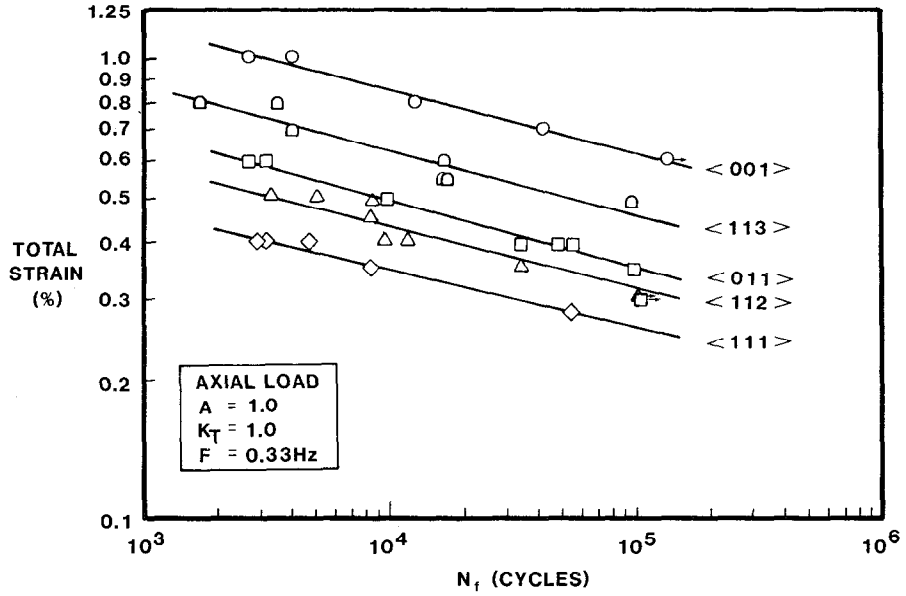

Figure 7 - Orientation Dependence of 1800°F Strain Controlled LCF Life of SC 7-14-6.

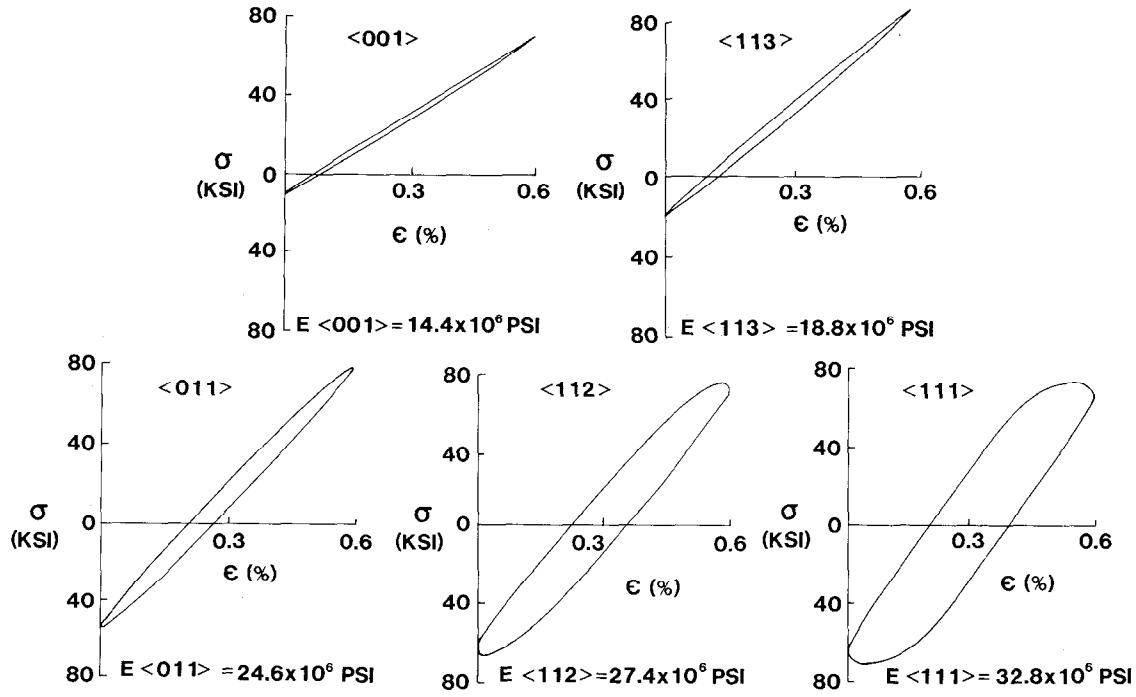

Figure 8 - Effect of Crystallographic Orientation on Fatigue Hysteresis at 1800°F and ε_T=0.6%.

Fatigue life was correlated with: 1) σ_M, the maximum tensile stress during test (23); 2) $\varepsilon_T E<hkl>$, the product of Young's Modulus (at

1800°F) and the total strain range (24); and 3) the Neuber parameter $\sqrt{\sigma_M \varepsilon_T E\langle hkl\rangle}$ (25). The fatigue life of the material is well described by either of the parameters which pertain to material modulus, Table VII, and is adequately characterized by $\varepsilon_T E\langle hkl\rangle$, Figure 9.

Table VII. Linear Regression Analysis of Fatigue Data

Dependent Variable	Independent Variable	Correlation Coefficient
log σ_M	log N_f	0.694
log $\varepsilon_T E\langle hkl\rangle$	log N_f	0.939
log $\sqrt{\sigma_M \varepsilon_T E\langle hkl\rangle}$	log N_f	0.947

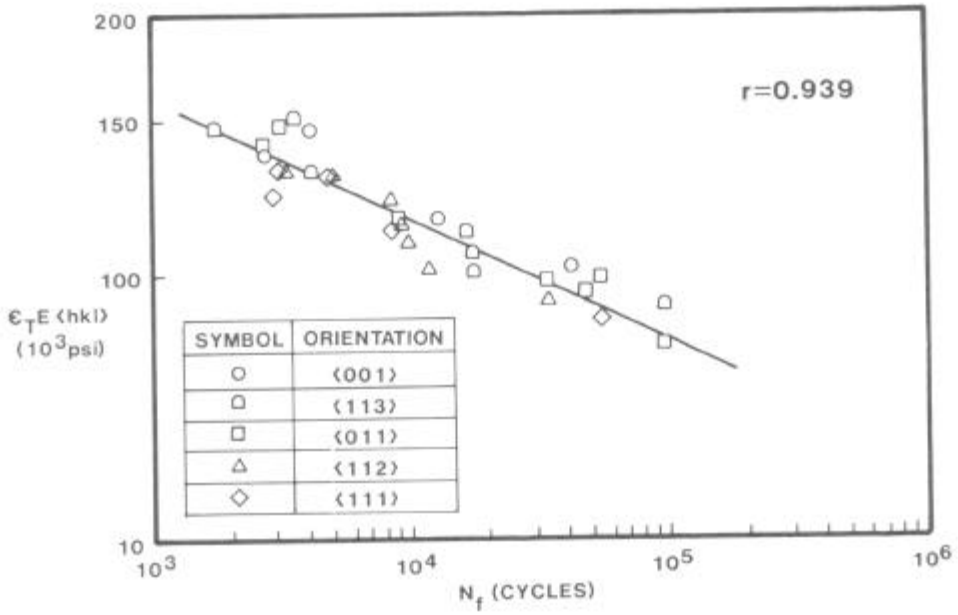

Figure 9 - 1800°F Strain Controlled LCF Life of SC 7-14-6.

SEM fractographic examination of failed test bars indicated that fatigue failure usually initiates in regions of surface or subsurface microporosity as expected (26), Figure 10.

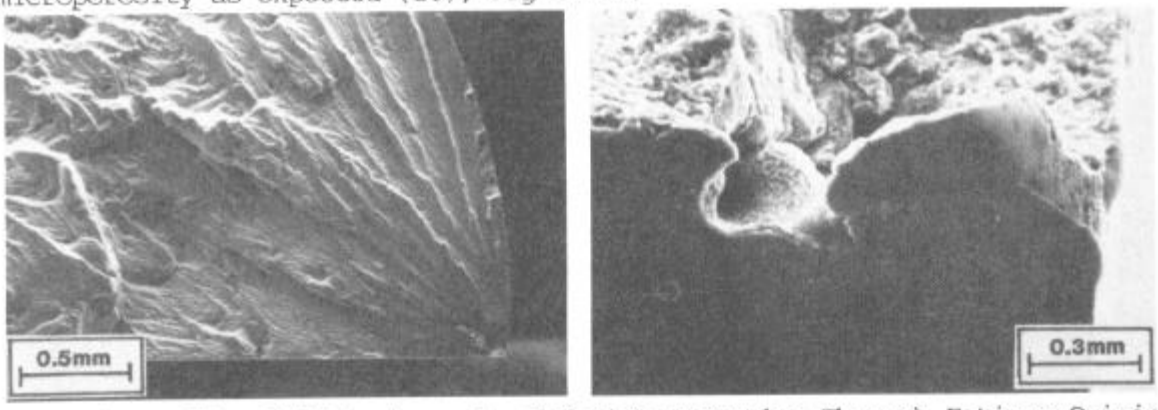

Figure 10 - SEM Fractograph of Polished Section Through Fatigue Origin in Failed ⟨011⟩ LCF Test Specimen.

Conclusions

Investment cast Ni-6.8Al-13.8Mo-6W alloy single crystals demonstrate a high degree of elevated temperature creep-rupture and fatigue strength anisotropy. The orientation dependence of fatigue strength correlates well with simple parameters based on Young's Modulus.

Acknowledgements

The authors would like to thank Mr. Larry Cash for conducting the fatigue testing, Prof. Orville Hunter (Iowa State University) for performing the dynamic modulus evaluations, Prof. Bruce Pletka (Michigan Technological University) for assisting with the lattice parameter measurements, Dr. Evan Ohriner (Climax Molybdenum Corp.) for doing the DTA studies, and Ms. Rebecca MacKay (NASA-Lewis) for her helpful discussions.

References

1. B.H. Kear, and B.J. Piearcy, "Tensile and Creep Properties of Single Crystals of the Nickel-Base Superalloy Mar-M200", Trans. TMS-AIME, 239 (1967) pp1209-1215.

2. F.L. VerSnyder and M.E. Shank, "The Development of Columnar Grain and Single Crystal High Temperature Materials Through Directional Solidification", Mat. Sci. Eng., 6 (1970), pp213-247.

3. B.J. Piearcey, U.S. Patent No. 3,494,709 (1970).

4. M. Gell, D.N. Duhl, and A.F. Giamei, "The Development of Single Crystal Superalloy Turbine Blades", Superalloys 1980, (1980), pp297-306.

5. J.E. Northwood, "Improving Turbine Blade Performance by Solidification Control", Metallurgia, (1979), pp437-442.

6. R.A. MacKay, R.L. Dreshfield, and R.D. Maier, "Anisotropy of Nickel-Base Superalloy Single Crystals", Superalloys 1980, (1980) pp385-394.

7. R.J. Patterson, A.R. Cox, and E.C. Van Reuth, "Rapid Solidification Rate Processing and Application of Turbine Engine Materials", Journal of Metals, (1980), pp34-39.

8. R.A. MacKay and L.J. Ebert, "The Development of Directional Coarsening of the γ' Precipitate in Superalloy Single Crystals", Scripta Met., (17), (1983), pp1217-1221.

9. D.D. Pearson, F.D. Lemky, and B.H. Kear, "Stress Coarsening of γ' and Its Influence on Creep Properties of a Single Crystal Superalloy", Superalloys 1980, (1980), pp513-520.

10. D.D. Pearson, B.H. Kear, and F.D. Lemky, "Factors Controlling the Creep Behavior of a Nickel-Base Superalloy", pp213-233 in Creep and Fracture of Engineering Materials and Structures, B. Wilshire and D.R.J. Owen, Eds; Prineridge Press, Swansea, UK, 1981.

11. P.W. Bridgman, U.S. Patent No. 1,793,672 (1931).

12. M.H. O'Brien, O. Hunter, Jr., M.D. Rasmussen, and H.D. Skank, "Digitally Controlled Measurement of Sonic Elastic Moduli and Internal Friction by Phase Analysis", Rev. Sci. Instru., 11(54), (1983), pp1565-1568.

13. R.F.S. Hearmon, An Introduction to Applied Anisotropic Elasticity, p25, Oxford University Press, Oxford, 1961.

14. D.H. Maxwell, "The Development of an Advanced Turbine Vane Alloy", Met. Eng. Quarterly, (1970), pp42-54.

15. J.F. Nye, Physical Properties of Crystals, Oxford University Press, Oxford, 1951.

16. Howmet Turbine Components Corporation Technical Bulletin TB 1075, 1979.

17. G. Simmons and H. Wang, Single Crystal Elastic Constants and Calculated Aggregate Properties: A Handbook, The MIT Press, Cambridge, Mass., 1971.

18. G.R. Leverant, and B.H. Kear, "The Mechanism of Creep in Gamma Prime Precipitation Hardened Nickel-Base Alloys at Intermediate Temperatures", Met. Trans., 1(2), (1970), pp491-498.

19. B.H. Kear, G.R. Leverant, and J.M. Oblak, "An Analysis of Creep-Induced Intrinsic/Extrinsic Fault Pairs in a γ' Precipitation Hardened Nickel-Base Alloy", Trans. ASM, 62, (1969), pp639-650.

20. G.R. Leverant, B.H. Kear, and J.M. Oblak, "Creep of Precipitation Hardened Nickel-Base Alloy Single Crystals at High Temperatures", Met. Trans., 4(1), (1973), pp355-362.

21. G.R. Leverant and D.N. Duhl, "The Effect of Stress and Temperature on the Extent of Primary Creep in Directionally-Solidified Nickel-Base Superalloys", Met. Trans., 2(3), (1971), pp907-911.

22. R.A. McKay and R.D. Maier, "The Influence of Orientation on the Stress Rupture Properties of Nickel-Base Superalloy Single Crystals", Met. Trans., (13A), (1982), pp1747-1754.

23. P.K. Wright and A.F. Anderson, "The Influence of Orientation on the Fatigue of Directionally-Solidified Superalloys", Superalloys 1980, (1980), pp689-698.

24. A.E. Gemma, B.S. Langer, and G.R. Leverant, "TMF Crack Propagation in an Anisotropic (Directionally-Solidified) Nickel-Base Superalloy", Thermal Fatigue of Materials and Components, ASTM STP 612 (1976), pp199-213.

25. B.M. Wundt, "Neuber's Relationship Between Stress and Strain Concentration Factors and Application of Low Cycle Fatigue", Effect of Notches in Low Cycle Fatigue, A Literature Survey, ASTM STP 490, (1972).

26. G.R. Leverant and M. Gell, "The Elevated Temperature Fatigue of a Nickel-Base Superalloy, Mar-M200, in Conventionally-Cast and Directionally-Solidified Forms", Trans. AIME, 245, (1969), pp1167-1173.